Results in Physics 22 (2021) 103857

Contents lists available at ScienceDirect

Results in Physics

journal homepage: www.elsevier.com/locate/rinp

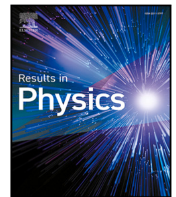

Crystalline growth and alloying of $In_xGa_{1-x}Sb$ films by electrodeposition onto liquid metal electrodes

Z.R. Lindsey *, M. Moran, P. Jacobson, Q. Smith, M.D. West, P. Francisco

Berry College, Rome, GA 30149, United States of America

A B S T R A C T

Incorporating indium (In) atoms into the GaSb lattice provides broad tunability of the optical bandgap within the infrared spectral region. This research documents the first instance in the literature of electrochemical liquid–liquid–solid (ec-LLS) growth of a ternary semiconductor alloy. Indium content of deposited $In_xGa_{1-x}Sb$ samples was regulated by controlling the Ga/In ratio of the liquid metal electrode. All depositions were performed using a single-step growth method under ambient pressure at 90 ± 5 °C. X-ray diffraction analysis showed shifts of the (111) diffraction peaks toward the peak locations of cubic InSb for the $x = 0.50$, 0.60, and 0.70 samples, indicating a consistent increase in lattice parameter. However, the $x = 0.28$ and 0.41 samples displayed unexpected shifts toward larger angles, possibly due to increased presence of Ga vacancies and antisites caused by Ga-rich growth conditions, as well as insufficient mixing of the liquid metal electrode for $x < 0.50$. Optical bandgaps ranging from 0.594 to 0.707 eV were determined via the Tauc method and Kubelka–Munk theory applied to diffuse reflectance data, and showed general agreement with measured lattice constants. Data obtained in this research supports In incorporation into the GaSb lattice for samples with $x \geq 0.50$, but with significantly lower In compositions relative to the liquid metal electrode. No general trend was observed for average crystallite size as a function of In composition, likely due to inconsistencies in the film harvesting process. This research provides further support for ec-LLS as a semiconductor growth technique capable of crystalline growth and alloying of III-V semiconductors.

Introduction

Semiconductors are critical to many aspects of modern technology due to desirable electronic and optical characteristics that are determined by material properties such as crystal structure and elemental composition. Gallium antimonide (GaSb) is a direct band gap III-V binary semiconductor with various optoelectronic [1–3] and energy conversion applications [4,5]. By strategically incorporating In atoms into the GaSb lattice to produce the ternary alloy $In_xGa_{1-x}Sb$, the optical bandgap can be tuned across the near infrared (NIR) and mid-infrared (mid-IR) regions of the electromagnetic spectrum from 1.7 μm to 7.3 μm [6]. This broad tunability accommodates further applications in infrared sensing and detection, environmental monitoring, data communications, bioimaging, and thermovoltaics [7–10].

However, the most common deposition processes for producing high-quality, crystalline semiconductors such as $In_xGa_{1-x}Sb$ include molecular beam epitaxy (MBE), liquid phase epitaxy (LPE), organometallic vapor phase epitaxy (OMVPE), and various other methods that all require high-cost, high-energy laboratory setups and involve the use of toxic precursors and/or extreme experimental conditions [11–14]. Electrodeposition is an alternative semiconductor deposition method that eliminates the necessity of high-cost experimental setups, hazardous precursors, or extreme pressures [15]. However, conventional electrodeposition methods pose several barriers to producing semiconductors of high crystal quality, displaying amorphous growth at temperatures below 500 °C (without additional thermal treatments), high impurity densities, and a lack of precise stoichiometric control and uniformity throughout deposited films of binary, ternary, and quaternary semiconductor systems [16–19].

The growth technique utilized in this research employs a hybrid deposition method that takes advantage of the simple experimental requirements associated with conventional electrodeposition, but with the addition of a liquid metal electrode that serves several functional roles that contribute to increased crystal quality of as-grown samples [20]. The growth method, called electrochemical liquid–liquid–solid (ec-LLS), was first realized by Carim et al. [21] and involves the use of a liquid metal electrode to simultaneously drive the electroreduction of compounds in solution and act as a growth platform for the resulting semiconductor crystals [22]. Having emerged over the past few years, ec-LLS has already displayed crystalline growth of Ge, Si, GaAs, GaSb, and InSb using low-cost, benchtop setups operated under ambient pressure and near room temperature [20–24].

This research tests the hypothesis that crystalline $In_xGa_{1-x}Sb$ thin films can be grown and alloyed in a controllable manner via ec-LLS by modifying the elemental composition of the liquid metal working electrode (WE). By varying the Ga/In mass ratio of the WE, the resulting as-grown crystalline $In_xGa_{1-x}Sb$ samples were characterized to determine In incorporation through various crystallographic and optical

* Corresponding author.
E-mail address: zlindsey@berry.edu (Z.R. Lindsey).

https://doi.org/10.1016/j.rinp.2021.103857
Received 8 January 2021; Accepted 14 January 2021
Available online 22 January 2021
2211-3797/© 2021 The Authors. Published by Elsevier B.V. This is an open access article under the CC BY-NC-ND license (http://creativecommons.org/licenses/by-nc-nd/4.0/).

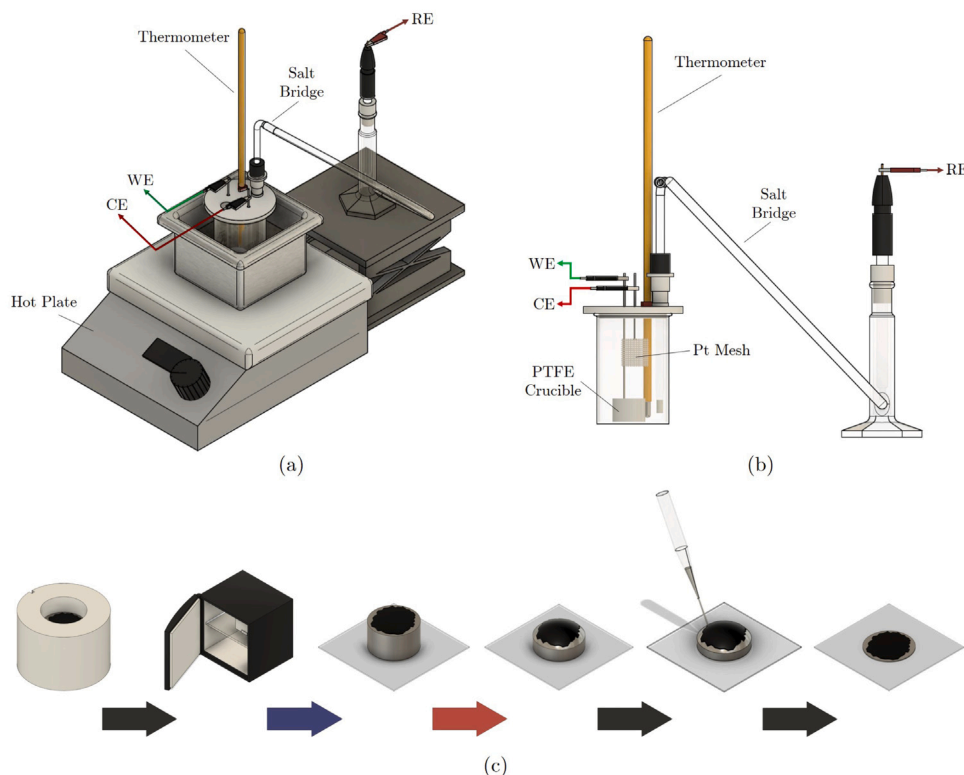

Fig. 1. Schematics depicting (a) overhead and (b) lateral views of ec-LLS growth setup used in this work, and (c) step-by-step sequence of film harvesting process.

spectroscopy techniques. X-ray diffraction (XRD) was performed to probe various crystal parameters and observe crystallographic changes as a function of In composition of the WE. In addition, diffuse reflection measurements were obtained via absorption spectroscopy to observe shifts in the optical bandgap as the In content of the WE was varied. This collective data was analyzed to quantify the degree of In incorporation into the GaSb lattice and to observe changes in crystal quality and optical bandgap as a result of the variation in In content.

Experimental details

Gallium (99.99%) and indium (99.9999%) used in the liquid metal electrode were obtained from Gallant Metals and Alfa Aesar, respectively. Platinum wire (99.95%) for making connections to the working and counter electrodes in solution was obtained from Surepure Chemetals, and a platinum mesh (≥99.9%; ~2 cm^2) used for the counter electrode was obtained from VWR. For the precursor and electrolyte, Sb_2O_3 (99.999%) and anhydrous NaOH (≥98%) were obtained from Sigma-Aldrich. Water used throughout all depositions had a quoted resistivity of >18.2 MΩ cm and was sourced from a Labconco Water Pro Plus purification system.

The electrochemical cell fabricated for this research was based on a similar setup used in the work of DeMuth et al. [23] but was modified slightly to accommodate a simpler, more maintenance-free design. As shown in Fig. 1, the growth cell uses a three-electrode configuration with the working and counter electrodes housed inside of a 150 mL Pyrex beaker. During growth, the Ga/In liquid metal WE is seated inside of a custom-made polytetrafluoroethylene (PTFE) crucible. Platinum wire (isolated via PTFE heat-shrink tubing) was used to make electrical contact to both the counter and working electrodes inside solution. In order to make electrical contact with the liquid metal WE, the platinum wire enters the PTFE crucible from underneath in order to minimally disturb semiconductor film growth at the top surface of the liquid metal. A single junction Al/AlCl reference electrode (RE) was connected to the growth cell via a salt bridge to prevent film contamination from the RE fill solution. The beaker was capped with a custom PTFE lid and then placed inside of an aluminum sand bath for increased heat retention. The deposition temperature was regulated via a hot plate and glass thermometer.

Deposition parameters for all films grown in this research were based off of a recent study conducted by DeMuth et al. on crystalline GaSb growth [23]. Electric stimuli were applied across the growth cell via a Gamry 1010E potentiostat. For all depositions, the liquid metal WE was held at a constant potential of −1.47 V (vs the Ag/AgCl RE) for 60 min in chronoamperometric mode, and the deposition temperature was maintained at 90 ± 5 °C throughout depositions. The bias voltage was applied across the cell just before submerging the CE and WE assembly into the prepared aqueous electrolyte/precursor solution (0.6 M NaOH; 0.1 mM Sb_2O_3) to discourage oxidation of the liquid metal. After the deposition process was completed, the PTFE crucible was removed from the growth cell and placed in a freezer as a preliminary step to film harvesting.

One major obstacle of ec-LLS as a thin film deposition process is the curvature of the liquid metal electrode. Not only does the curvature of the liquid metal surface inhibit large-scale sample growth, but it also adds difficulty to the process of preserving the integrity of the semiconductor layer during film harvest. As depicted in Fig. 1, once the PTFE crucible containing the thin film atop the liquid metal electrode is removed from the growth cell, it is placed in a freezer to allow the liquid metal to solidify. Once the liquid metal has solidified, the crucible is removed from the freezer and briefly warmed with a heat gun to the point where the solid metal pellet is able to be removed from the crucible. The metal pellet is then placed onto a glass slide with the film facing upwards and heated until the underlying metal again enters the liquid state. In the final step, the underlying liquid metal is removed via a glass pipet, resulting in a thin film ready for analysis and/or further treatments. While this process results in a reasonably flat film to the naked eye, it became clear from XRD analysis (discussed in ‘Results and Discussions’) that the surface flatness achieved with the

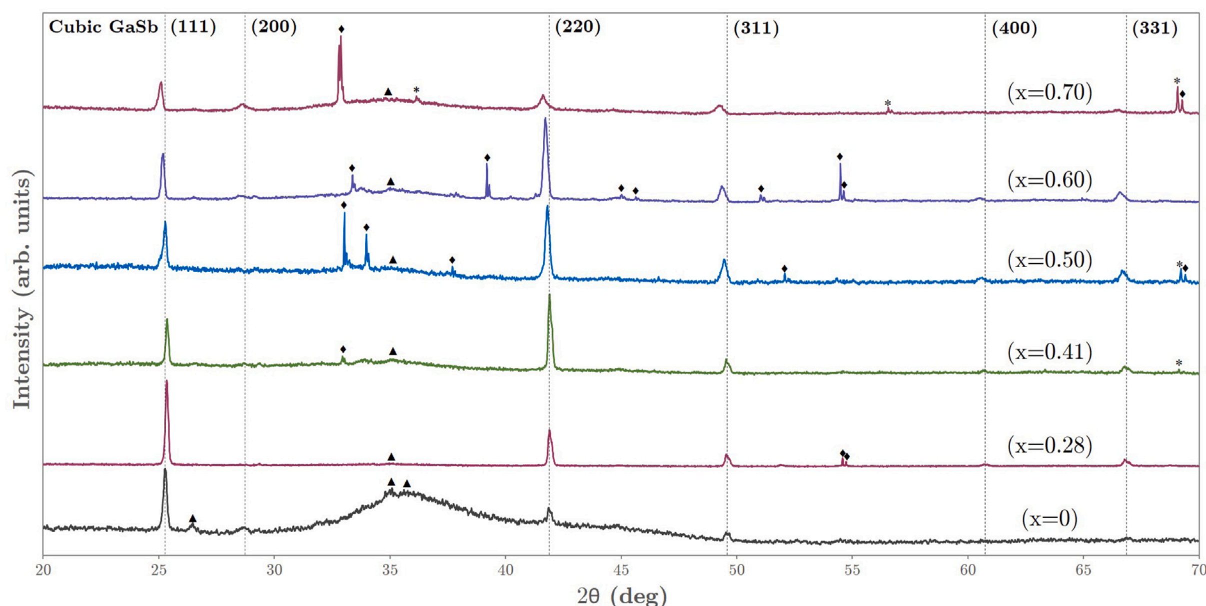

Fig. 2. Stacked XRD powder scan data showing measured diffraction peaks for cubic $In_xGa_{1-x}Sb$ samples (compared to cubic GaSb peak locations indicated by dashed lines), crystalline Ga (cubic phase indicated by ∗ and orthorhombic phase indicated by ⧫), and amorphous Ga_2O_3 (indicated by ▴).

harvesting method described above requires improvement before ec-LLS can be considered for optoelectronic material synthesis for device applications.

In order to test the plausibility of using ec-LLS to produce a ternary alloy via a single-step growth process, the Ga/In ratio of the liquid metal electrode was varied for multiple depositions. While all other deposition parameters were kept constant, depositions were performed with various In_xGa_{1-x} liquid metal compositions (x = 0, 0.28, 0.41, 0.50, 0.60, 0.70) of the WE. To achieve these compositions, the appropriate masses of Ga and In were weighed and placed into the PTFE crucible. Immediately after the bias voltage was applied to the electrodes across the cell, the assembly was lowered into the electrolyte/precursor solution to initiate the deposition process.

X-ray diffraction was performed on all samples via a Panalytical Empyrean multipurpose diffractometer in powder scan mode. Diffuse reflectance measurements were obtained for optical bandgap characterization via a Jasco V670 UV–VIS–NIR spectrophotometer with 150 mm integrating sphere.

Results and discussion

Powder XRD measurements were obtained to determine crystal phase, average crystallite size, and lattice constant as a function of In composition of the WE. Full XRD powder scan plots for samples grown with In_xGa_{1-x} WE compositions of x = 0, 0.28, 0.41, 0.50, 0.60, and 0.70 are displayed in Fig. 2. Diffraction peak centroids were determined from XRD data, and Bragg's Law was used to obtain measured values for the lattice constant of all samples. Bragg's Law is given by

$$2d_{hkl}sin\theta = n\lambda, \quad (1)$$

where d_{hkl} is the interplanar spacing, λ is the K-alpha$_1$ X-ray wavelength (1.540598 Å), n is an integer, and θ is the angle between incident X-rays and a crystal plane (i.e. measured 2θ diffraction angle divided by 2). After determining d_{hkl} using Eq. (1), measured values for the lattice constant were determined using

$$d_{hkl} = \frac{a}{\sqrt{h^2 + k^2 + l^2}}, \quad (2)$$

where h, k, and l are the Miller indices of a given crystal plane and a is the lattice constant. Fig. 3 shows a more detailed view of observed shifts of the (111) diffraction peak for all samples.

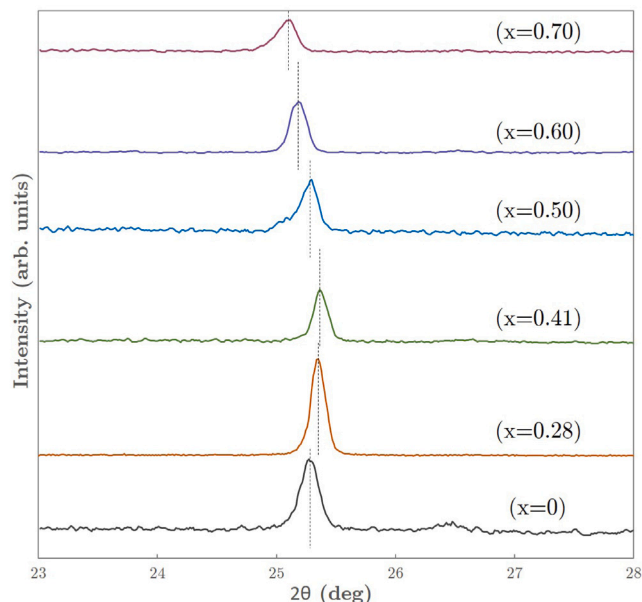

Fig. 3. Stacked XRD powder scan data of (111) diffraction peaks showing shifts associated with increased In composition of In_xGa_{1-x} liquid metal electrode.

The lattice constant of cubic GaSb (6.0959 Å) should increase and approach that of cubic InSb (6.4974 Å) as more In is incorporated into the cubic crystal lattice [25]. As the In content of the WE is increased, diffraction peaks should be observed to shift to smaller angles toward the peak locations of cubic InSb to confirm In-alloying of deposited samples. This behavior was consistently observed for the x = 0.50, 0.60, and 0.70 samples, resulting in respective lattice constant measurements of 6.1071 Å, 6.1231 Å, and 6.1497 Å, which correspond to actual In concentrations of x = 0.03, 0.07, and 0.14 (according to Vegard's law [26] calculations). Conversely, the x = 0.28 and x = 0.41 samples exhibited unexpected shifts of the (111) diffraction peak to slightly higher angles (complete XRD data listed in Table 1). One feasible explanation for these unexpected shifts observed for the x = 0.28 and

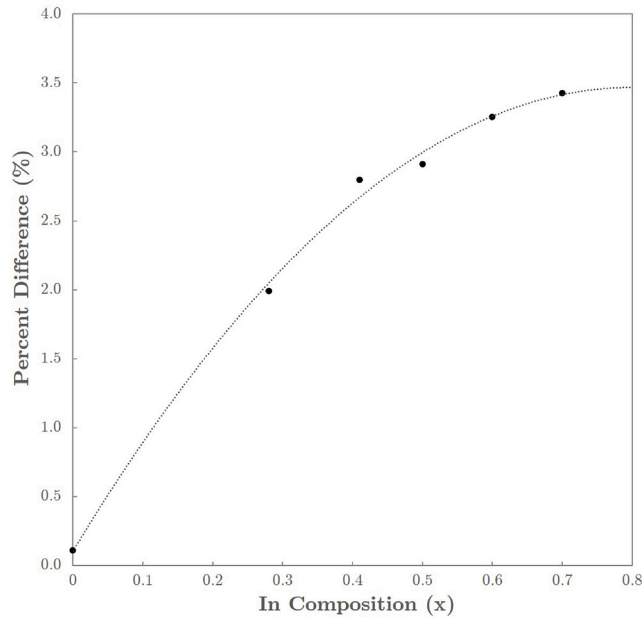

Fig. 4. Percent difference between nominal and measured lattice constants of as-grown samples as a function of In composition (x) of In_xGa_{1-x} liquid metal electrode.

x = 0.41 samples is an excess of native acceptor species such as Ga vacancies (V_{Ga}) and Ga antisites (Ga_{Sb}) in samples grown under Ga-rich conditions [27,28]. These crystal defects exhibit sub-bandgap absorption and have been shown to be effectively compensated through the incorporation of metallic species such as beryllium and tellurium into the GaSb lattice [27–30]. While XRD features attributed to amorphous Ga_2O_3 were found in all samples, the most prominent Ga_2O_3 features were generally found in samples with higher Ga/In ratios (x < 0.50) in the liquid metal electrode, which could have also contributed to the unexpected shifts observed for low x samples. Due to the presence of residual Ga beneath harvested thin film samples, diffraction peaks associated with cubic and orthorhombic phases of metallic Ga are observed in XRD data for all samples.

Another probable cause for the disparities observed for the $x = 0.28$ and $x = 0.41$ samples is the preparation of the In_xGa_{1-x} liquid metal electrode for these samples. Contamination of the liquid metal electrode was a significant concern throughout experiments, so interaction with the liquid metal mixture was minimized in attempts to discourage contamination. Since Ga becomes liquid at ~30 °C, the $x = 0$ sample was prepared by heating a Ga-filled vial via a hot water bath before insertion into the PTFE crucible. For the $x = 0.28$ and $x = 0.41$ samples, the Ga was prepared in the same way, and appropriate masses of In shot were simply dropped into the Ga melt and allowed to dissolve without any mechanical mixing. For samples with higher In content ($x \geq 0.50$), the Ga/In mixtures were heated in a Pyrex beaker (to accommodate increased melting points with increasing x) and gently swirled before transferring to the PTFE crucible. As an overall trend observed for all samples, the In composition was greatly reduced in deposited samples compared to that of the In_xGa_{1-x} liquid metal electrode. Additionally, as the In composition of the liquid metal electrode was increased, the disparity between nominal and measured lattice constants of deposited samples displayed a small but nontrivial increase with increasing x (shown in Fig. 4). All data obtained in this research supports the significance of full incorporation of the Ga/In species within the liquid metal electrode, resulting in more effective preservation of the stoichiometry from the liquid metal electrode to deposited semiconductor samples.

Measured values for average crystallite size in the (111) growth direction were determined using the Scherrer equation [31,32], given

Table 1
Experimental data and relevant measured quantities related to determination of lattice constant ($a_{measured}$), average crystallite size (D_{111}), and optical bandgap (E_g) for all samples as the In content (x) of the liquid metal working electrode was varied. XRD data listed in this table were obtained from the (111) diffraction peak.

x (mol. frac.)	$2\theta_{Bragg}$ (deg)	$a_{measured}$ (Å)	$a_{nominal}$ (Å)	$\Delta a_{measured}$ (Å)	FWHM (deg)	D_{111} (nm)	E_g (eV)	ΔE_g (eV)
0	25.257	6.1025	6.0959	0.0037	0.381	21.381	0.669	0.012
0.28	25.349	6.0809	6.2032	0.0018	0.144	56.377	0.698	0.024
0.41	25.351	6.0804	6.2530	0.0019	0.315	38.760	0.707	0.013
0.50	25.238	6.1071	6.2875	0.0054	0.748	10.877	0.662	0.026
0.60	25.171	6.1231	6.3258	0.0036	0.171	47.687	0.621	0.006
0.70	25.060	6.1497	6.3641	0.0036	0.289	28.173	0.594	0.011

by

$$D_{hkl} = \frac{K\lambda}{B_{hkl}cos\theta}, \quad (3)$$

where D_{hkl} is the average crystallite size in the direction perpendicular to the hkl lattice plane, K is the crystallite shape factor [33] (K= 0.9 was used in this work), λ is the X-ray wavelength, B_{hkl} is the full-width at half-maximum (FWHW) of the hkl diffraction peak (in radians), and θ is the Bragg angle. While the $x = 0.28$ sample was determined to have the largest average crystallite size of 56.377 nm, no general trend was observed as a function of In content. This lack of an observed relationship between crystallite size and In incorporation is most likely due to the variability in the film harvesting process discussed in the previous section and further supports the necessity to refine post-growth harvesting methods.

Because of inhibited transmission due to the presence of a thin layer of residual liquid gallium underneath harvested thin film samples, diffuse reflectance measurements were performed to determine the optical bandgap of all samples. Diffuse reflectance measurements were converted to corresponding absorption spectra via the Kubelka–Munk function [34], given by

$$F(R_\infty) = \frac{(1-R_\infty)^2}{2R_\infty} = \alpha, \quad (4)$$

where R_∞ is the reflectance of an "infinitely thick" sample (ie. no contributions from supporting background). This commonly used approximation is widely accepted [35,36] and allows for $F(R_\infty)$ to be substituted for absorption (α) in the equation utilized in the Tauc method determination of optical bandgap [37], given by

$$(\alpha h\nu)^{1/n} = C(h\nu - E_g), \quad (5)$$

where h is Planck's constant, ν is the photon frequency (in Hz), C is a proportionality constant, E_g is the bandgap, and n is a parameter based on the electronic transition of the semiconductor bandgap. To determine the appropriate value of n, direct allowed transitions require $n = \frac{1}{2}$ (which is the case for GaSb and InSb), while $n = 2$ is used for indirect allowed transitions, $n = \frac{2}{3}$ is used for direct forbidden transitions, and $n = \frac{1}{3}$ is used for indirect forbidden transitions [38,39]. Combining Eqs. (4) and (5) for $n = \frac{1}{2}$ yields

$$[F(R_\infty)h\nu]^2 = C(h\nu - E_g), \quad (6)$$

and plotting $[F(R_\infty)h\nu]^2$ against the photon energy ($h\nu$) allows a measured value of the bandgap to be determined from the x-intercept of the linear fit at the absorption edge.

Using this approach, Fig. 5 shows plots corresponding to each sample with determined values for the optical bandgap. While the abruptness of the absorption edge varied from sample to sample, distinct linear regions were identified and linear fits (indicated by the red dashed lines in Fig. 5) were performed for each sample. At room temperature, the documented bandgap of GaSb is 0.680 eV [40], which is a 1.63% difference from the measured value of 0.669 ± 0.012 eV

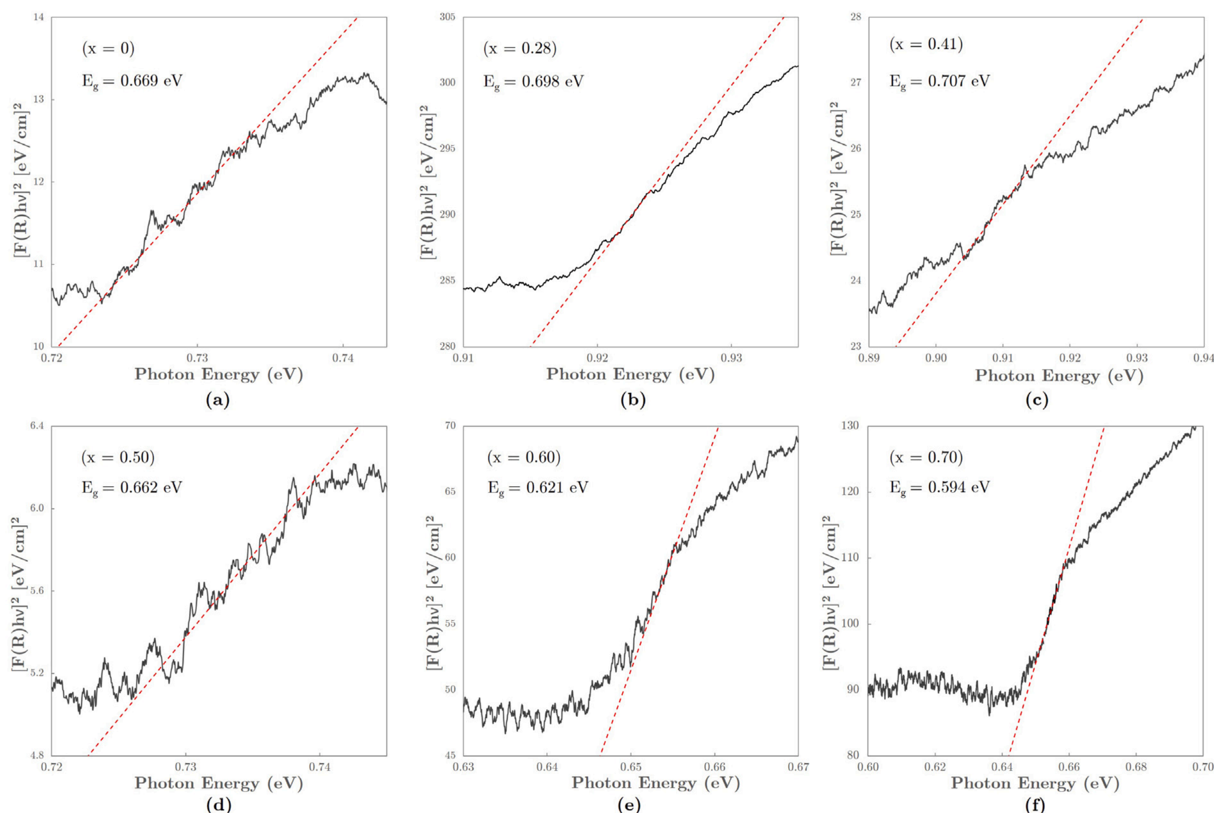

Fig. 5. Tauc plots produced via Kubelka–Munk approximation and diffuse reflectance measurements showing measured bandgaps determined from linear fits at the absorption edge for samples grown with (a) $x = 0$, (b) $x = 0.28$, (c) $x = 0.41$, (d) $x = 0.50$, (e) $x = 0.60$, and (f) $x = 0.70$ for the In_xGa_{1-x} liquid metal electrode.

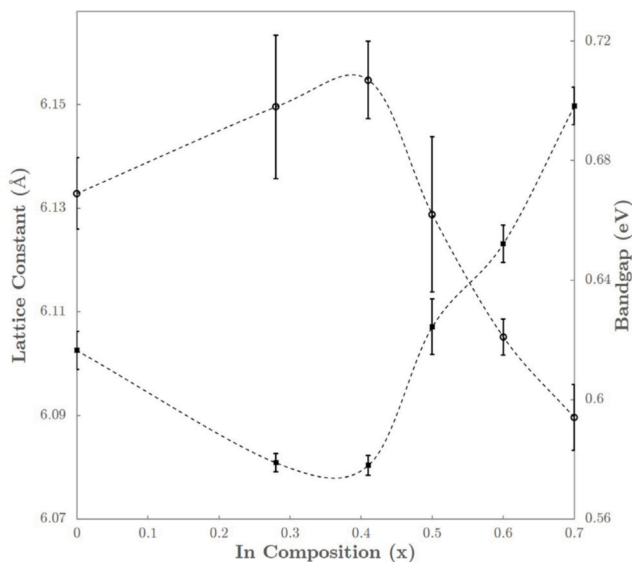

Fig. 6. Measured values of lattice constant (indicated by ■) and optical bandgap (indicated by ∘) as a function of In composition of In_xGa_{1-x} liquid metal electrode.

determined for the $x = 0$ sample. Assuming increased In incorporation into the GaSb lattice with increasing x of the liquid metal electrode, the bandgap is expected to decrease and approach the documented bandgap of InSb at room temperature, which is 0.17 eV [40]. Even though a consistent decrease in bandgap was not observed with increasing In composition of the liquid metal electrode, the measured bandgap values mirrored the general trend observed in lattice constant measurements determined from XRD data (as shown in Fig. 6). These results are consistent with the notion that reduced atomic spacing within a crystal generally results in an increased energy gap between the valence and conduction bands. Uncertainties in bandgap and lattice constant measurements were determined using standard error analysis methods and are reported in Table 1 and Fig. 6 (via error bars).

Conclusions

This research documents the first instance of successful crystalline growth of a ternary semiconductor alloy by means of the ec-LLS deposition method. Several alloyed compositions of polycrystalline $In_xGa_{1-x}Sb$ were deposited using an in-house, benchtop ec-LLS setup, with all depositions performed under ambient pressure at 90 ± 5 °C in an electrolyte solution of 0.6 M NaOH with a precursor of 0.1 mM Sb_2O_3. Shifts of the (111) diffraction peak for the x = 0.50, 0.60, and 0.70 samples were observed, displaying clear shifts toward smaller Bragg angles as the In composition was increased. However, the x = 0.28 and 0.41 samples displayed shifts in the (111) diffraction peak to larger angles than that of cubic GaSb, which was an unexpected result. Possible explanations for the unexpected shifts include increased presence of Ga vacancies (V_{Ga}), Ga antisites (Ga_{Sb}), and amorphous Ga_2O_3 for samples grown under Ga-rich conditions, as well as insufficient mixing of the In_xGa_{1-x} liquid metal electrode for samples with $x <$ 0.50. While measured values of lattice constant and optical bandgap support In incorporation into the GaSb lattice for the x = 0.50, 0.60, and 0.70 samples, the actual In compositions of deposited samples were determined to be significantly lower than that of the corresponding prepared liquid metal electrodes. The disparity between the In composition of the liquid metal electrode and deposited semiconductor samples showed an increasing trend with increasing x of the In_xGa_{1-x} liquid metal electrode. Measured values for the average crystallite size of samples varied from 10.877 to 56.377 nm, but no general trend was

observed as a function of In composition of deposited samples, likely due to non-ideal film harvesting methods.

Diffuse reflectance data was obtained, and measured values for the optical bandgap were determined via the Tauc method and Kubelka–Munk approximation. Bandgap measurements ranged from 0.594 to 0.707 eV and showed general agreement with the measured values for lattice constant determined from XRD data. It is evident from XRD analysis that the resulting In composition of as-grown samples is significantly lower than that of the corresponding liquid metal electrodes. However, for depositions where the liquid metal electrode solution was heated during the mixing process, the resulting deposited semiconductor samples showed convincing evidence of In-alloying, both from measurements of lattice constant and optical bandgap.

This study shows promise for the extension of using ec-LLS to produce and alloy several other crystalline ternary and quaternary semiconductor materials, and targeted improvements in the crystal quality and alloying process could potentially be realized with appropriate revisions to the presented methods of mixing the liquid metal electrode before deposition, as well as post-deposition film harvesting methods. Otherwise, ec-LLS continues to emerge as a capable, low-cost, benchtop semiconductor growth technique, operating under ambient pressure and near room temperature.

CRediT authorship contribution statement

Z.R. Lindsey: Conceptualization, Methodology, Formal Analysis, Resources, Writing - original draft, Visualization, Supervision, Project administration, Funding acquisition. **M. Moran:** Conceptualization, Methodology, Investigation, Data curation. **P. Jacobson:** Conceptualization, Methodology, Investigation, Data curation. **Q. Smith:** Conceptualization, Methodology, Investigation. **M.D. West:** Investigation, Data curation. **P. Francisco:** Conceptualization, Methodology.

Declaration of competing interest

The authors declare that they have no known competing financial interests or personal relationships that could have appeared to influence the work reported in this paper.

Data availability:

The data that supports the findings of this study are available within the article. However, additional data support is available from the corresponding author upon reasonable request.

Acknowledgments

The authors acknowledge the Richards Science Scholars, United States of America, Synovus, United States of America, and Summer Undergraduate Research Fellowship, United States of America grants, as well as the Berry College Office of Undergraduate Research, United States of America for financial support of this research. XRD was performed at the University of Alabama at Birmingham at the UAB Material Growth and Characterization Service Center.

References

[1] Milnes AG, Polyakov AY. Gallium antimonide device related properties. Solid-State Electron 1993;36:803.

[2] Dutta PS, Sangunni KS, Bhat HL, Kumar V. Experimental determination of melt-solid interface shapes and actual growth rates of gallium antimonide grown by vertical Bridgman method. J Cryst Growth 1994;141:476.

[3] Motosugi G, Kagawa T. Temperature dependence of the threshold current of AlGaAsSb/GaSb DH lasers. Japan J Appl Phys 1980;19:2303.

[4] Juang BC, Laghumavarapu RB, Foggo BJ, Simmonds PJ, Lin A, Liang B, et al. GaSb thermophotovoltaic cells grown on GaAs by molecular beam epitaxy using interfacial misfit arrays. Appl Phys Lett 2015;106:111101.

[5] Fraas LM, Girard GR, Avery JE, Arau BA, Sundaram VS, Thompson AG, et al. GaSb booster cells for over 30% efficient solar cell stacks. J Appl Phys 1989;66:3866.

[6] Wolenski C, Zhang W, Meyer C, Triplett G, Cole N. Composition and surface deformation variance in highly strained $In_xGa_{1-x}Sb$ structures on (100) GaSb. J Vac Sci Technol A 2016;34:21403.

[7] Refaat TF, Abedin MN, Bhagwat V, Bhat IB, Dutta PS, Singh UN. InGaSb photodetectors using an InGaSb substrate for 2 μm applications. Appl Phys Lett 2004;85:1874.

[8] Grein CH, Young PM, Flatté ME, Ehrenreich H. Long wavelength InAs/InGaSb infrared detectors: Optimization of carrier lifetimes. J Appl Phys 1995;78:7143.

[9] Li D, Yip S, Li F, Zhang H, Meng Y, Bu X, et al. Flexible near-infrared InGaSb nanowire array detectors with ultrafast photoconductive response below 20 μs. Adv Opt Mater 2020;8:2001201.

[10] Wang CA, Choi HK, Ransom SL, Charache GW, Danielson LR, DePoy DM. High-quantum-efficiency 0.5 eV GaInAsSb/GaSb Thermophotovoltaic devices. Appl Phys Lett 1999;75:1305.

[11] Segawa K, Otsubo M, Miki H, Fujibayashi K. $Ga_xIn_{1-x}Sb$ crystals grown by liquid phase epitaxy. Japan J Appl Phys 1978;17:165.

[12] Roslund JH, Zsebök O, Swenson G, Andersson TG. Molecular beam epitaxy growth and characterization of $Ga_xIn_{1-x}Sb$ on GaAs substrates. J Cryst Growth 1997;175/176:883.

[13] Ehsani H, Bhat I, Gutmann RJ. Role of relative tilt on the structural properties of GaInSb epitaxial layers grown on (001) GaSb substrates. J Appl Phys 1999;86:835.

[14] Kaneko T, Asahi H, Okuno Y, Gonda S. MOMBE (Metalorganic Molecular Beam Epitaxy) growth of InGaSb on GaSb. J Cryst Growth 1989;95:158.

[15] Abedin SZE, Endres F. Electrodeposition of metals and semiconductors in air- and water-stable ionic liquids. Chem Phys Chem 2006;7:58.

[16] Paolucci F, Mengoli G, Musiani MM. An electrochemical route to GaSb thin films. J Appl Electrochem 1990;20:868.

[17] Yang M, Landau U, Angus JC. Electrodeposition of GaAs from aqueous electrolytes. J Electrochem Soc 1992;39:3480.

[18] McChesney JJ, Haigh J, Dharmadasa I, Mowthorpe D. Electrochemical growth of GaSb and InSb for applications in infra-red detectors and optical communication systems. Opt Mater 1996;6:63.

[19] Chung Y, Lee C. Electrochemically fabricated alloys and semiconductors containing indium. J Electrochem Sci Technol 2012;3:95.

[20] Gu J, Fahrenkrug E, Maldonado S. Direct electrodeposition of crystalline silicon at low temperatures. J Am Chem Soc 2013;135:1684.

[21] Azhar CI, Collins SM, Foley JM, Maldonado S. Benchtop electrochemical liquid–liquid–solid growth of nanostructured crystalline germanium. J Am Chem Soc 2011;133:13292.

[22] Fahrenkrug E, Gu J, Maldonado S. Electrodeposition of crystalline GaAs on liquid gallium electrodes in aqueous electrolytes. J Am Chem Soc 2013;135:330.

[23] DeMuth J, Ma L, Fahrenkrug E, Maldonado S. Electrochemical liquid-liquid-solid deposition of crystalline gallium antimonide. Electrochim Acta 2016;197:353.

[24] Fahrenkrug E, Rafson J, Lancaster M, Maldonado S. Concerted electrodeposition and alloying of antimony on indium electrodes for selective formation of crystalline indium antimonide. Langmuir 2017;33:9280.

[25] Swaminathan V, Macrander AT. Materials aspects of GaAs and InP based structures. Prentice Hall; 1991.

[26] Vegard L. The constitution of mixed crystals and the space occupied by atoms. Z Phys 1921;5:17.

[27] Chandola A, Pino R, Dutta PS. Below bandgap optical absorption in tellurium-doped GaSb. Semicond Sci Technol 2005;20:886.

[28] Baxter RD, Bate RT, Reid FJ. Ion-pairing between lithium and the residual acceptors in GaSb. J Phys Chem Solids 1965;26:41.

[29] Wang D, Lui X, Tang J, Fang X, Fang D, Li J, et al. Optical Properties improvement of GaSb epilayers through defects compensation via doping. J Lumin 2017;197:266.

[30] Hidalgo P, Mendez B, Piqueras J, Dutta PS, Dieguez E. Effect of In doping in GaSb crystals studied by cathodoluminescence. Semicond Sci Technol 1999;14:901.

[31] Scherrer P. Determination of the size and the internal structure of colloidal particles by means of X-rays. Göttinger Nachr Math Phys 1918;2:98.

[32] Holzwarth U, Gibson N. The Scherrer equation versus the 'Debye-Scherrer equation'. Nature Nanotech 2011;6:534.

[33] Klug HP, Alexander LE. X-ray diffraction procedures. 2nd ed. Wiley; 1974.

[34] Kubelka F, Munk F. A contribution to the optics of pigments. Z Techn Phys 1931;12:593.

[35] Zanatta AR. Revisiting the optical bandgap of semiconductors and the proposal of a unified methodology to its determination. Sci Rep 2019;9:11225.

[36] Murphy AB. Band-gap determination from diffuse reflectance measurements of semiconductor films, and application to photoelectrochemical water-splitting. Sol Energy Mater Sol Cells 2007;91:1326.

[37] Tauc J, Grigorovici R, Vancu A. Optical properties and electronic structure of amorphous germanium. Phys Status Solidi 1966;15:627.

[38] Makuła P, Pacia M, Macyk W. How to correctly determine the band gap energy of modified semiconductor photocatalysts based on UV–vis spectra. J Phys Chem Lett 2018;9:6814.

[39] Escobedo-Morales A, Ruiz-López I, Ruiz-Peralta M, Tepech-Carrillo L, Sánchez-Cantú M, Moreno-Orea J. Automated method for the determination of the band gap energy of pure and mixed powder samples using diffuse reflectance spectroscopy. Heliyon 2018;5:2405.

[40] Kittel C. Introduction to solid state physics. 6th ed. Wiley; 1986.